Research Square

Preprints are preliminary reports that have not undergone peer review.
They should not be considered conclusive, used to inform clinical practice,
or referenced by the media as validated information.

p300-mediated H3K18la activation of IDO1 transcription promotes immune evasion of ovarian cancer to MSLN-KIR CAR-T cells

Su Wang
Nanjing Medical University
Zitong Shen
Nanjing Medical University
Yuchen Huang
Nanjing Medical University
Yongqian Shu
Nanjing Medical University
Tongpeng Xu
tongpeng_xu_njmu@163.com
Nanjing Medical University
Yanhong Gu
Nanjing Medical University

Research Article

Keywords:

Posted Date: November 25th, 2026

DOI: https://doi.org/10.21203/rs.3.rs-11611525/v1

License: This work is licensed under a Creative Commons Attribution 4.0 International License.
Read Full License

Additional Declarations: No competing interests reported.

Abstract

Background

For advanced multidrug-resistant ovarian cancer, the MSLN-KIR chimeric antigen receptor T (CAR-T) cells previously developed by our team have demonstrated clinical potential; however, treatment resistance remains a critical bottleneck. This study aimed to elucidate the mechanisms underlying this resistance and to identify potential strategies to enhance CAR-T efficacy.

Methods

We performed single-cell RNA sequencing on tumor tissues from ovarian cancer patients before and after MSLN-KIR CAR-T infusion to identify key genes associated with treatment resistance. In vitro functional assays, chromatin immunoprecipitation, and co-immunoprecipitation were conducted to explore the regulatory axis. The therapeutic efficacy of combined inhibitors was evaluated using in vivo xenograft models in NCG mice.

Results

Indoleamine 2,3-dioxygenase 1 (IDO1) was identified as a key metabolic gene mediating resistance. In vitro experiments confirmed that IDO1 depleted CAR-T cell cytotoxicity and cytokine secretion, while its metabolic product, kynurenine (KYN), dose-dependently suppressed CAR-T function and induced apoptosis. Mechanistically, lactate accumulation in the tumor microenvironment drove p300-catalyzed histone H3K18 lactylation (H3K18la). This modification enriched at the IDO1 promoter region and initiated its transcription. Animal experiments demonstrated that combined inhibition of IDO1 and p300 effectively alleviated tumor resistance to MSLN-KIR CAR-T therapy and significantly reduced tumor burden.

Conclusions

Our findings elucidate a novel mechanism by which ovarian cancer evades MSLN-KIR CAR-T immunity through the lactate-p300-H3K18la-IDO1 axis. Targeting this pathway with p300 and IDO1 inhibitors provides a viable combined therapeutic strategy to overcome CAR-T resistance in ovarian cancer.

1. Introduction

Ovarian cancer is the gynecologic malignancy with the highest mortality rate, with more than 300,000 new cases and approximately 200,000 deaths worldwide each year [1]. As early symptoms are insidious, most patients are already at an advanced stage when diagnosed and have a poor prognosis [2]. Although surgery combined with paclitaxel plus platinum-based chemotherapy can achieve a relatively

high initial response rate, most patients ultimately have a poor prognosis due to recurrence and drug resistance [3, 4]. In addition, although poly(ADP-ribose) polymerase (PARP) inhibitors have demonstrated clear efficacy in the treatment of advanced recurrent ovarian cancer, their significant survival benefit has mainly been established in the subgroup of patients carrying BRCA1/BRCA2 mutations, which accounts for only about 10% to 16% of all patients with ovarian cancer [5–8]. In recent years, immune checkpoint inhibitors have achieved breakthroughs in multiple solid tumors; however, in ovarian cancer, the objective response rate with monotherapy remains very limited, suggesting that the immunosuppressive microenvironment is a key bottleneck limiting the efficacy of immunotherapy [9–12]. Therefore, developing novel immunotherapeutic strategies and elucidating the mechanisms of immune escape in ovarian cancer are clinically important for improving patient prognosis.

CAR-T therapy is one of the most revolutionary breakthroughs in tumor immunotherapy. It mainly involves introducing antigen-specific chimeric antigen receptors (CARs) into patient-derived T cells via gene transfer, followed by in vitro selection, expansion, and intravenous reinfusion into patients, thereby exerting a tumor-killing effect [13, 14]. It has shown marked efficacy in hematologic malignancies such as B-cell acute lymphoblastic leukemia and diffuse large B-cell lymphoma [15–18]. However, CAR-T therapy still faces many challenges in solid tumors, including antigen heterogeneity, insufficient T-cell infiltration, and functional exhaustion mediated by the immunosuppressive microenvironment [19–22]. Critically, conventional CARs rely on the CD3ζ chain to transduce activation signals, whereas CD3ζ in the solid tumor microenvironment is susceptible to inhibitory signals and shows downregulated phosphorylation, leading to insufficient CAR-T activation and functional exhaustion, thereby compromising the therapeutic efficacy of CAR-T cells in solid tumors [23, 24].

To improve the survival rate of patients with advanced multidrug-resistant ovarian cancer and to address the bottlenecks of conventional CAR structures in clinical application for ovarian cancer, CAR-T cells with a structure distinct from conventional CARs were previously designed to enhance therapeutic efficacy. Our research group previously designed a multi-chain CAR structure in which a KIR/DAP12 complex replaces CD3ζ, and demonstrated that this structure can enhance the antitumor efficacy of CAR-T cells [25, 26]. Meanwhile, we selected the ovarian cancer marker mesothelin (MSLN) as the targeting antigen; previous studies have reported that MSLN-targeted CAR-T cells have shown promising efficacy against ovarian cancer [27]. Based on the above results, we designed MSLN-targeted KIR/DAP12-based CAR-T cells (MSLN-KIR CAR-T cells), and have initiated a clinical trial (ChiCTR2100046544.May 21, 2021) to verify the safety and efficacy of these cells in treating patients with ovarian cancer [28]. However, some patients still experience treatment resistance, which has become a key issue limiting the clinical application of this therapy. Therefore, we aim to explore the mechanisms underlying resistance to CAR-T cell therapy, with the goal of improving the efficacy of CAR-T cell therapy for ovarian cancer.

To enable CAR-T cells to exert potent antitumor effects, the functional constraints imposed by the tumor microenvironment must be overcome as much as possible. Metabolic reprogramming in the tumor microenvironment has become a major focus of tumor immunology research in recent years. Tumor cells commonly exhibit enhanced aerobic glycolysis—the Warburg effect—resulting in substantial lactate

accumulation in the microenvironment [29, 30]. Long regarded as a metabolic waste product, lactate is now recognized as a signaling molecule that can promote immune evasion through multiple mechanisms [31–33]. Lactate suppresses effector cells such as CD8 + T cells and NK cells, supports immunosuppressive cells such as Tregs and MDSCs, and contributes to immune dysfunction through epigenetic reprogramming, HIF-1α stabilization, NF-κB activation, and other signaling pathways [34]. Notably, lactate-driven histone lactylation—a novel post-translational modification identified in 2019—directly links metabolic state to gene transcription [35]. This modification has been shown in multiple tumors to regulate immune-related gene expression and contribute to microenvironment remodeling; however, whether and how it affects CAR-T efficacy in ovarian cancer remains poorly understood [36, 37].

Indoleamine 2,3-dioxygenase 1 (IDO1) is the rate-limiting enzyme in tryptophan metabolism along the kynurenine pathway. It is highly expressed in multiple tumors and creates an immunosuppressive microenvironment by depleting local tryptophan and accumulating kynurenine (KYN) [38, 39]. Previous studies have reported that IDO1 is associated with resistance to various immunotherapies [40]. However, the role of IDO1 in MSLN-KIR CAR-T therapy in ovarian cancer and its upstream regulatory mechanisms have not yet been reported. In particular, whether lactate regulates IDO1 expression through epigenetic modifications and thereby affects CAR-T efficacy remains unclear.

In this context, this study systematically investigated the molecular mechanisms underlying resistance to this therapy in ovarian cancer by analyzing single-cell transcriptome data from ovarian cancer patients before and after MSLN-KIR CAR-T treatment, together with in vitro functional experiments and animal models. We identified IDO1 as a key gene contributing to treatment resistance, validated the inhibitory effect of the IDO1/KYN metabolic axis on CAR-T function, and further revealed a novel epigenetic regulatory axis, lactate–p300–H3K18la–IDO1, providing a potential combination therapeutic strategy for improving CAR-T efficacy in ovarian cancer.

2. Materials and Methods

2.1 Clinical samples and ethical statement

Patients with ovarian cancer who received MSLN-KIR CAR-T therapy at the First Affiliated Hospital of Nanjing Medical University were enrolled in this study (ChiCTR2100046544). Tumor tissue samples were obtained before and at specific time points after CAR-T cell infusion for single-cell sequencing. In accordance with the clinical trial protocol, informed consent was obtained from all participants in the clinical trial. Participants did not receive compensation for participating in the clinical trial. This trial was approved by the institutional review boards of the participating centers, and all patients provided written informed consent.

2.2 Single-cell RNA sequencing

Ovarian cancer tissues were enzymatically digested to prepare single-cell suspensions. Cell counting and viability were assessed using a Countess II Automated Cell Counter with trypan blue staining. Prior

to loading, the cell concentration was required to be at least 700 cells/μL, with a viability exceeding 80%. The cell suspension, barcoded gel beads, and partitioning oil were then loaded onto a 10x Genomics Chromium chip to form single-cell gel bead-in-emulsions (GEMs). Within the GEMs, cells were lysed, and the released mRNA underwent reverse transcription to synthesize cDNA tagged with cell barcodes. Following PCR amplification of the reverse transcription products, scRNA-seq libraries were constructed using the Chromium Next GEM Single Cell 5' Reagent Kits v2.0 (PN-1000395 and PN-1000352) and sequenced on an Illumina NovaSeq 6000 platform to generate 2 × 150 bp paired-end reads. Raw data were aligned to the human reference genome GRCh38 using Cell Ranger (v5.0.0) to obtain the single-cell gene expression matrices for each sample.

Prior to cell clustering using the Seurat R package (v3.1.1), stringent quality control was performed to retain high-quality cells. First, doublets were identified and removed for each sample using DoubletFinder, followed by further filtering based on the number of detected genes, total unique molecular identifiers (UMIs), and the proportion of mitochondrial gene expression. Cells expressing 200 to 7,800 genes, with fewer than 56,000 UMIs and a mitochondrial gene percentage of less than 25%, were retained for subsequent analysis. The filtered expression matrices were normalized using the LogNormalize method, and Harmony was employed for data integration and batch effect correction.

2.3 Cell culture and treatment

Human ovarian cancer cell lines OVCAR-3 and SK-OV-3 were purchased from KeyGEN BioTECH. OVCAR-3 cells were cultured in RPMI-1640 medium supplemented with 20% FBS, 10 μg/mL insulin, and 1% penicillin/streptomycin. SK-OV-3 cells were cultured in McCoy's 5A medium supplemented with 10% FBS and 1% penicillin/streptomycin. All cells were maintained at 37°C in a humidified atmosphere containing 5% CO_2. Cell lines were authenticated by STR profiling and confirmed to be free of mycoplasma contamination.

2.4 CAR-T cell preparation and culture

MSLN-KIR CAR-T cells were manufactured by Nanjing CART Medical Technology Co., Ltd. Peripheral blood mononuclear cells were isolated from the subjects by density gradient centrifugation (Ficoll-Paque). The isolated T cells were activated with anti-CD3/CD28 stimulation in medium containing IL-2. After 24 h, the cells were transduced with a lentiviral vector encoding the MSLN-KIR CAR (composed of an anti-MSLN single-chain variable fragment [scFv] fused to a KIR/DAP12 multi-chain signaling domain). Transduced CAR-T cells were maintained and expanded in IL-2-containing medium. After a specific culture period, the cells were harvested for subsequent experiments. Prior to in vitro assays, the CAR expression positivity rate on the T cell surface was determined by flow cytometry.

2.5 Transfection and transduction

siRNAs targeting IDO1 (si-IDO1) and p300 (si-p300), as well as negative control siRNA (si-NC), were purchased from OBiO Technology (Shanghai) Corp., Ltd. The siRNA sequences were verified by BLAST to ensure no off-target effects. For transient knockdown, siRNAs (final concentration 50 nM) were

transfected into OVCAR-3 and SK-OV-3 cells using Lipofectamine RNAiMAX. For overexpression, the full-length cDNA of IDO1 was amplified by PCR and cloned into the pcDNA3.1(+) vector. The overexpression plasmid or empty vector control was transfected into ovarian cancer cells using Lipofectamine 3000. To establish stable knockdown cell lines, tumor cells were transduced with lentivirus carrying IDO1-targeting shRNA (sh-IDO1) or negative control shRNA (sh-NC), followed by puromycin selection. The sequences are listed in Table S1.

2.6 RNA extraction and quantitative real-time PCR (qRT-PCR)

Total RNA was extracted from cells using RNA-easy Isolation Reagent (Vazyme, R701-01, China). A total of 1 μg RNA was reverse-transcribed using HiScript III RT SuperMix for qPCR (+ gDNA wiper) (Vazyme, R323-01, China). The cDNA was then amplified using Taq Pro Universal SYBR qPCR Master Mix (Vazyme, Q712-02, China). The relative expression levels were calculated using the 2^-ΔΔCt method, with β-tubulin as the internal reference. The primer sequences are listed in Table S1.

2.7 Western blotting and antibodies

Cells were lysed on ice for 30 min using RIPA lysis buffer (Beyotime, P0013C, China) supplemented with protease inhibitors (Biosharp, BL612A, China) and phosphatase inhibitors (Beyotime, P1082, China). The lysates were centrifuged at 12,000 × g for 15 min at 4°C, and the supernatants were collected. Protein concentration was determined using a BCA assay. For tumor tissues, the tissues were first thoroughly minced, lysed with the lysis buffer, and sonicated; the subsequent steps were the same as described above. A total of 20 μg protein (40 μg for tissue lysates) was separated by SDS-PAGE and transferred to a PVDF membrane. The membranes were blocked with 5% non-fat milk at room temperature for 2 h and incubated with primary antibodies overnight at 4°C. After washing three times with TBST, the membranes were incubated with HRP-conjugated secondary antibodies for 1 h at room temperature. Signals were visualized using ECL, and the band intensities were quantified using ImageJ software, with β-tubulin or total H3 as the internal reference. The antibodies used included anti-IDO1 (Proteintech, 66528-1-Ig, China), anti-p300 (Proteintech, 83078-5-RR, China), anti-Pan Kla (PTM BIO, PTM-1401RM, China), anti-H3K18la (PTM BIO, PTM-1406RM, China), anti-H3K9la (PTM BIO, PTM-1419RM, China), anti-H3K14la (PTM BIO, PTM-1414RM, China), anti-H3K27la (PTM BIO, PTM-1428RM, China), anti-H3K56la (PTM BIO, PTM-1421RM, China), anti-Histone H3 (Proteintech, 68503-1-Ig, China), and anti-Tubulin (Servicebio, ZB15140-HRP, China).

2.8 Cytotoxicity assay

To evaluate the killing effect of CAR-T cells on different target cells, tumor cells were seeded into 96-well plates at a density of 1 × 10^4 cells/well and allowed to adhere overnight. The next day, CAR-T cells were added at an effector-to-target (E:T) ratio of 1:1 and co-cultured for 24 h. CCK-8 and LDH assays were used to detect the cytotoxicity of CAR-T cells against tumor cells. In addition, to investigate the effect of KYN on CAR-T cell cytotoxicity, CAR-T cells were treated with different concentrations of KYN, and then CAR-T cells or UTD cells were co-cultured with tumor cells at various E:T ratios for CCK-8 assay. For the

CCK-8 assay, 10 μL of CCK-8 reagent (Beyotime, C0038, China) was added to each well and incubated at 37°C in the dark for 2–4 h, and the absorbance was measured at 450 nm. For the LDH assay, the lactate dehydrogenase cytotoxicity assay kit (Beyotime, C0016, China) was used to measure the LDH release in the supernatant, and the absorbance was measured at 490 nm.

2.9 ELISA

Specific ELISA kits were used to detect the concentrations of IFN-γ, IL-2, TNF-α, and KYN in the supernatant. The quantitative kits for IFN-γ, IL-2, and TNF-α were purchased from BioLegend (USA), and the KYN quantitative kit was purchased from RUIXIN BIOTECH (China). The procedures were performed according to the manufacturer's instructions, and the optical density (OD) values were read at 450 nm.

2.10 Apoptosis assay

To investigate the effect of KYN on CAR-T cell apoptosis, activated CAR-T cells were treated with different concentrations of KYN and then stained with an Annexin V-FITC/PI apoptosis detection kit (KeyGEN BioTECH, KGA1102, China). The apoptosis rate was analyzed by flow cytometry.

2.11 Immunofluorescence

Cell coverslips were placed at the bottom of 24-well plates, and cells were seeded onto the coverslips. The cells were fixed with 4% paraformaldehyde at room temperature for 15 min, permeabilized with 0.5% Triton X-100 for 10 min, and then blocked with 5% goat serum at room temperature for 30 min. Primary antibodies were added and incubated overnight at 4°C. After washing with PBS, the cells were incubated with Alexa Fluor 488- and 594-conjugated secondary antibodies for 1 h at room temperature in the dark. Nuclei were counterstained with DAPI. Images were acquired using a confocal fluorescence microscope and analyzed for mean fluorescence intensity using ImageJ software.

2.12 Co-immunoprecipitation (Co-IP)

Cells were lysed in lysis buffer containing protease inhibitors at 4°C for 30 min. The lysates were centrifuged at 12,000 × g for 15 min, and the supernatants were collected. A portion of the supernatant was saved as the input, while the remaining supernatant was incubated with primary antibodies overnight at 4°C with rotation. Protein A/G magnetic beads were then added and incubated at 4°C for 4 h. After washing the beads, the immunoprecipitated complexes were eluted by boiling in 2× SDS loading buffer at 95°C for 10 min. The eluates were subjected to Western blot analysis, with IgG used as a negative control.

2.13 Chromatin immunoprecipitation (ChIP)

The ChIP assay was performed using the ChIP Assay Kit with Protein A/G Magnetic Beads (Beyotime, P2080S, China) according to the manufacturer’s instructions. Briefly, OVCAR-3 or SK-OV-3 cells were cross-linked with 1% formaldehyde, collected, lysed, and sonicated to shear the DNA. The DNA-protein complexes were then isolated by incubation with a ChIP-grade anti-H3K18la antibody (PTM BIO, PTM-1427RM, China) or isotype control IgG. Protein A/G magnetic beads were added to the lysates and

incubated at 4°C for 2 h. After elution from the beads, the DNA fragments were reverse cross-linked at 65°C for 4 h and purified using a DNA purification kit (Beyotime, D0033, China). The purified DNA was analyzed by quantitative PCR.

2.14 Animal experiments

Female NCG mice (6–8 weeks old, purchased from GemPharmatech Co., Ltd., Nanjing, China) were housed in an SPF-grade barrier facility and acclimated for 1 week before the experiments. SK-OV-3 cells stably transduced with sh-NC or sh-IDO1 (1×10^7 cells) were subcutaneously inoculated into the right flank of the mice. Seven days after inoculation, when tumor formation was confirmed, the mice were randomly divided into two groups (n = 6 per group). MSLN-KIR CAR-T cells (5×10^6 cells per mouse) were injected via the tail vein. Tumor length (L) and width (W) were measured every 3 days, and tumor volume was calculated using the formula $V = (L \times W^2) / 2$. At the end of the experiment, the mice were euthanized, and the tumors were excised and weighed.

For the combination therapy model, SK-OV-3 cells were subcutaneously inoculated into mice, and after tumor formation, the mice were randomly divided into five groups (n = 6 per group): UTD group, CAR-T group, CAR-T + IDO1i group, CAR-T + p300i group, and CAR-T + IDO1i + p300i group. The IDO1 inhibitor epacadostat (50 mg/kg) was administered via intraperitoneal injection every 3 days, and the p300 inhibitor C646 (15 mg/kg) was administered via intraperitoneal injection every 2 days. CAR-T cells were injected via the tail vein. Tumor volume was monitored regularly. At the end of the experiment, the mice were euthanized, and the tumors were excised and weighed for subsequent analysis. The experimental endpoint was defined as a body weight loss exceeding 20% of the initial weight, loss of mobility, or ulceration within the tumor. At the end of the experiment, mice were euthanized by CO_2 inhalation. The CO_2 chamber was slowly filled at a displacement rate of 20% of the chamber volume per minute to ensure a gradual loss of consciousness. Euthanasia was confirmed by cervical dislocation following respiratory arrest.

2.15 HE staining and immunohistochemistry

The excised tumor tissues were fixed in 4% paraformaldehyde for 24 h, followed by routine gradient ethanol dehydration, xylene clearing, and paraffin embedding. Tissue sections (4 μm) were deparaffinized in xylene and rehydrated through a graded ethanol series before undergoing HE staining and immunohistochemical analysis.

For HE staining, the sections were stained with hematoxylin for 5 min, rinsed with running water, differentiated with acid ethanol, and counterstained with eosin for 2 min. After dehydration and mounting, images were captured under a microscope.

For Ki-67 immunohistochemistry, the sections were subjected to antigen retrieval using citrate buffer (pH 6.0) at 95°C for 20 min. After blocking endogenous peroxidase with 3% H_2O_2 and blocking non-specific binding with 5% BSA, the sections were incubated with anti-Ki-67 antibody overnight at 4°C. The next day, the sections were incubated with HRP-conjugated secondary antibody, visualized using DAB, and

counterstained with hematoxylin. After dehydration and mounting, the sections were observed and imaged under a microscope.

2.16 Statistical analysis

All in vitro experiments were independently repeated at least three times, and each in vivo group contained at least six mice ($n \geq 6$). Data are presented as mean ± SD. Comparisons between two groups were performed using Student's *t*-test, while comparisons among multiple groups were performed using one-way or two-way analysis of variance (ANOVA). A P value of < 0.05 was considered statistically significant. Statistical analyses were conducted using GraphPad Prism 9.0 and R software.

3. Results

3.1 IDO1 is associated with resistance to MSLN-KIR CAR-T therapy in ovarian cancer patients

To overcome the limitation that CD3ζ cannot effectively activate intracellular signaling during traditional CAR-T therapy for solid tumors, our group previously designed a novel MSLN-targeting CAR-T (MSLN-KIR CAR-T) for the treatment of ovarian cancer patients, which demonstrated significant efficacy. Meanwhile, we performed single-cell RNA sequencing on tumor tissue samples from patients before and after treatment. To investigate which genes in ovarian cancer cells may influence patient resistance to MSLN-KIR CAR-T therapy, we analyzed changes in tumor cell subpopulations and gene expression profiles in two ovarian cancer patients before and after CAR-T cell infusion. First, through dimensionality reduction and unsupervised clustering analysis of malignant cell populations before and after treatment, we identified seven cell clusters, and observed that the M3 cluster was significantly increased after treatment (**Fig. 1A-B,Fig. S1A**). These results suggested that the M3 cluster might be resistant to MSLN-KIR CAR-T-mediated killing. Next, we performed differential gene expression analysis on the M3 cluster before and after treatment (**Fig. 1C**), focusing primarily on genes upregulated after treatment. Simultaneously, we performed differential gene expression analysis on malignant cells from poor-responder patients before and after treatment (**Fig. 1D**), also focusing on upregulated genes. By intersecting the upregulated genes from these two gene sets, we identified seven differentially expressed genes. We analyzed the expression levels of these seven genes in ovarian cancer (**Fig. 1E-F**) and focused on three of them (CXCL10, IGKV3-11, and IDO1). Among them, IDO1 has been reported to be associated with CAR-T therapy resistance in other cancers. Therefore, we selected IDO1 for further investigation to explore whether it is associated with tumor cell resistance to MSLN-KIR CAR-T therapy in ovarian cancer.

Next, we performed in vitro experiments. First, MSLN-positive ovarian cancer cell lines OVCAR-3 and SK-OV-3 were selected, and IDO1 was knocked down using siRNA. RT-qPCR and Western blot analysis showed that IDO1 was significantly knocked down in the cells (**Fig. 1G-H**). Then, IDO1-knockdown and non-knockdown tumor cells were co-cultured with CAR-T cells for 24 h (effector-to-target ratio of 1:1). CCK-8 and LDH assays showed that knocking down IDO1 in tumor cells enhanced the cytotoxic effect of CAR-T cells (**Fig. 1I-J**). Meanwhile, we measured the concentrations of cytotoxic cytokines in the co-

culture supernatant. The results showed that co-culture with IDO1-knockdown tumor cells significantly increased the secretion of IFN-γ, IL-2, and TNF-α by CAR-T cells (**Fig. 1K-M**). Furthermore, after overexpressing IDO1 in OVCAR-3 and SK-OV-3 cells (**Fig. S1B**), the cytotoxic effect of CAR-T cells on tumor cells was attenuated (**Fig. S1C-D**), and the secretion of IFN-γ, IL-2, and TNF-α was reduced **(Fig. S1E-G**).

Subsequently, we inoculated sh-NC or sh-IDO1 SK-OV-3 cells into mice to establish xenograft models. Seven days after inoculation, when tumor formation was confirmed, CAR-T cells were infused, and tumor volume was regularly monitored thereafter. The results showed that the IDO1-knockdown group exhibited smaller tumor volume, lighter tumor weight, and better CAR-T therapeutic efficacy (**Fig. 1N-P**). In summary, these results indicate that IDO1 in ovarian cancer can lead to patient resistance to MSLN-KIR CAR-T therapy, and targeting IDO1 can significantly enhance the efficacy of CAR-T therapy for ovarian cancer.

3.2 IDO1 mediates KYN accumulation, and KYN suppresses CAR-T cell function

IDO1 has been widely reported to mediate the metabolism of tryptophan to kynurenine (KYN), and KYN can create an immunosuppressive tumor microenvironment, thereby affecting the function of immune cells. Correspondingly, GSEA enrichment analysis of differentially expressed genes in malignant cell populations from ovarian cancer patients before and after treatment showed an upward trend in the tryptophan metabolism pathway (**Fig. 2A**). Therefore, we aimed to investigate the effect of KYN on MSLN-KIR CAR-T cell therapy in ovarian cancer.

First, we observed that after 24 h, si-NC SK-OV-3 cells released approximately 1.12 μM of KYN, whereas KYN production was significantly reduced after IDO1 knockdown (**Fig. 2B**). Correspondingly, overexpression of IDO1 facilitated the conversion of more Trp to KYN (**Fig. 2C**). Next, MSLN-KIR CAR-T cells were treated with different concentrations of KYN and then co-cultured with tumor cells for 24 h. It was observed that compared with UTD cells, CAR-T cells exhibited a significantly stronger cytotoxic effect on tumor cells, whereas KYN treatment inhibited the killing effect of CAR-T cells in a dose-dependent manner **(Fig. 2D**). Meanwhile, as the concentration of KYN increased, the secretion of IFN-γ and IL-2 by CAR-T cells decreased (**Fig. 2E-F**). In addition, after CAR-T cells were treated with KYN for 2 days, Annexin-V / PI staining showed that the apoptosis rate of CAR-T cells gradually increased with the increase of KYN concentration (**Fig. 2G**). In summary, we conclude that the IDO1 metabolite KYN inhibits the function and activity of MSLN-KIR CAR-T cells.

3.3 H3K18la activates IDO1 expression in ovarian cancer

To investigate the mechanism regulating IDO1 gene expression in ovarian cancer, we further analyzed the single-cell data and performed GSEA enrichment analysis on differentially expressed genes in the M3 cluster from poor-responder ovarian cancer patients before and after treatment. We noticed a significant increase in the glycolysis pathway (**Fig. 3A**). Lactate is produced by glycolysis, and lactylation has been

reported to be associated with IDO1 in other disease models; however, whether lactylation regulates IDO1 in ovarian cancer remains unknown [41].

To investigate whether lactylation regulates IDO1 in ovarian cancer, we first treated OVCAR-3 cells with lactate and detected changes in pan-lactylation levels by Western blot analysis. It was observed that after lactate treatment, pan-lactylation levels were significantly increased, with the dominant protein band at 15–17 kDa, indicating that this protein was histone H3. We then examined antibodies against specific H3 lactylation sites and confirmed that H3K18la exhibited the most significant change (**Fig. 3B**). Therefore, we subsequently focused on the relationship between H3K18la and IDO1.

Glycolysis inhibitors 2-DG and oxamate can reduce intracellular lactate levels, whereas rotenone, as a mitochondrial electron transport chain complex inhibitor, can cause intracellular lactate accumulation and increase endogenous lactate (**Fig. 3C**). We treated OVCAR-3 and SK-OV-3 cells with the glycolysis inhibitors 2-DG and oxamate, and observed that with increasing doses, intracellular pan-lactylation and H3K18la levels gradually decreased (**Fig. 3D-E**). Next, chromatin immunoprecipitation was performed using an H3K18la antibody, and ChIP-qPCR demonstrated that H3K18la was enriched in the IDO1 promoter region, and this enrichment could be attenuated by glycolysis inhibitors (**Fig. 3F**). We then investigated the effect of H3K18la on IDO1 expression. As expected, after glycolysis inhibitor treatment, both the mRNA and protein levels of IDO1 decreased (**Fig. 3G-H**). In contrast, with the increase of exogenous and endogenous lactate, the protein levels of IDO1 increased **(Fig. 3I, Fig. S2A-B**). Meanwhile, we observed that the inhibitory effect of glycolysis inhibitors on IDO1 could be partially reversed by exogenous lactate (**Fig. 3J**). These results indicate that H3K18la positively regulates IDO1 transcription.

3.4 p300 positively regulates H3K18la in ovarian cancer

As a potential histone lactyltransferase, p300 has been reported to catalyze H3K18la in multiple cancer types [42, 43]. Therefore, we aimed to investigate whether p300 catalyzes H3K18la in ovarian cancer, thereby affecting IDO1 expression. Survival analysis using the GEPIA online database showed that high p300 expression was associated with poor prognosis in ovarian cancer **(Fig. 4A**).

To demonstrate the interaction between H3K18la and p300 in ovarian cancer, we first performed immunofluorescence assays, and the results showed that p300 and H3K18la co-localized in OVCAR-3 and SK-OV-3 cells (**Fig. 4B**). In addition, Co-IP also demonstrated binding between p300 and H3K18la in ovarian cancer (**Fig. 4C-D**). Subsequently, to investigate how p300 affects H3K18la expression in ovarian cancer, we treated ovarian cancer cells with a p300 inhibitor for 24 h and then detected H3K18la levels by Western blot analysis. It was observed that with increasing inhibitor concentrations, pan-lactylation and H3K18la levels decreased (**Fig. 4E**). Meanwhile, we knocked down p300 in OVCAR-3 and SK-OV-3 cells using siRNA. Western blot analysis showed that while p300 was knocked down, pan-lactylation and H3K18la levels were also significantly inhibited (**Fig. 4F**). Similarly, immunofluorescence showed that p300 knockdown reduced the fluorescence intensity of H3K18la (**Fig. 4G-H**).

3.5 p300 regulates IDO1 through catalyzing H3K18la

As the writer enzyme of H3K18la, p300 affects H3K18la expression in ovarian cancer, which may in turn affect the transcription of downstream factors of H3K18la. To verify whether p300 regulates IDO1 expression through catalyzing H3K18la, we performed ChIP-qPCR experiments. The results showed that after adding the p300 inhibitor, the binding of H3K18la to the IDO1 promoter region was significantly reduced, and this phenomenon could be partially reversed by lactate (**Fig. 5A**). Similarly, after p300 knockdown, the binding of H3K18la to the IDO1 promoter region was significantly decreased, and this binding could be upregulated by the addition of exogenous lactate (**Fig. 5B**). Therefore, p300 may upregulate IDO1 expression by enhancing H3K18la modification. RT-qPCR and Western blot analysis showed that after adding the p300 inhibitor or knocking down p300, both the transcriptional and translational levels of IDO1 were decreased (**Fig. 5C-E**). The addition of exogenous lactate could partially restore H3K18la and IDO1 expression (**Fig. 5F-G**). The above results indicate that p300 upregulates IDO1 expression through catalyzing H3K18la.

3.6 Combined use of IDO1i and p300i enhances the anti-tumor effect of MSLN-KIR CAR-T

To explore the possibility of reducing ovarian cancer resistance to MSLN-KIR CAR-T therapy, we investigated the effect of CAR-T combined with an IDO1 inhibitor or a p300 inhibitor on tumor growth. We selected epacadostat to inhibit IDO1, which is a selective inhibitor that specifically binds to the active site of IDO1. Next, SK-OV-3 cells were subcutaneously inoculated into mice, and then the mice were treated with UTD, CAR-T, CAR-T combined with IDO1 inhibitor (CAR-T + IDOi), CAR-T combined with p300 inhibitor (CAR-T + p300i), and CAR-T combined with IDO1 inhibitor and p300 inhibitor (CAR-T + IDO1i + p300i), respectively **(Fig. 6A**). We observed that compared with the CAR-T alone group, the CAR-T + IDOi and CAR-T + p300i groups exhibited smaller tumor volumes and lighter tumor weights, while the combination group (CAR-T + IDO1i + p300i) had the smallest tumor volume (**Fig. 6B-C**). Similarly, immunohistochemical staining showed that the combination group (CAR-T + IDO1i + p300i) significantly reduced the tumor growth rate (**Fig. 6D**). In addition, Western blot analysis of IDO1 in tumor tissues showed that the combination group (CAR-T + IDO1i + p300i) significantly reduced the expression level of IDO1 (**Fig. 6E**). The above results indicate that the combination of a p300 inhibitor and an IDO1 inhibitor can partially alleviate the resistance of ovarian cancer cells to MSLN-KIR CAR-T therapy.

4. Discussion

CAR-T therapy, as an emerging therapeutic approach for tumors, has been widely applied in the treatment of hematological malignancies; however, its application in solid tumors has encountered a bottleneck. Among these challenges, the complex tumor microenvironment is a major factor. To improve the survival rate of patients with advanced ovarian cancer, our group designed MSLN-KIR CAR-T cells with a structure distinct from conventional CARs to treat ovarian cancer. CAR structural design is a critical step in CAR-T cell therapy. The conventional CAR structure consists of three parts: an extracellular domain, a transmembrane domain, and an intracellular domain [44, 45]. The extracellular

domain comprises a variable region single-chain antibody that can bind to specific antigens on the tumor surface; we selected mesothelin as the targeted antigen. Mesothelin (MSLN) is a glycosylated phosphatidylinositol-anchored membrane glycoprotein that is abnormally elevated in ovarian cancer tissues and patient plasma, while its expression in normal tissues is extremely low or absent. Therefore, MSLN can serve as a tumor marker for ovarian cancer [46, 47]. The transmembrane domain connects the intracellular and extracellular regions and plays a role in signal transduction. The intracellular domain is mainly composed of CD3ζ and co-stimulatory factors, which can activate T cells. Conventional CAR activation of T cells relies on CD3ζ, and CD3ζ is susceptible to exhaustion induced by the tumor microenvironment [48, 49]. Therefore, our group optimized the CAR structure and innovatively designed a multi-chain CAR structure, namely a killer cell immunoglobulin-like receptor (KIR)/DNAX activation protein 12 (DAP12) structure replacing CD3ζ as the signal transduction component. This multi-chain immune receptor complex has been proven to enhance the killing effect of T cells on tumors. Meanwhile, we conducted an open-label clinical trial, demonstrating the safety and efficacy of MSLN-KIR CAR-T in treating ovarian cancer patients. Subsequently, to further explore the possibility of enhancing the therapeutic effect of MSLN-KIR CAR-T in ovarian cancer, we performed single-cell analysis on tumor tissues from patients before and after treatment.

By analyzing single-cell transcriptomic data of ovarian cancer before and after MSLN-KIR CAR-T cell therapy, combined with in vitro functional experiments and mouse xenograft models, we found that IDO1 may be involved in ovarian cancer resistance to MSLN-KIR CAR-T therapy, and we proposed for the first time the p300-H3K18la-IDO1 axis in ovarian cancer. The results suggest that lactate-related epigenetic regulation may weaken the anti-tumor function of MSLN-KIR CAR-T cells by promoting IDO1 expression and kynurenine accumulation. Furthermore, combined inhibition of IDO1 and p300 further enhanced the anti-tumor effect of CAR-T cells in mouse models, providing a potential research direction for improving the efficacy of CAR-T therapy for ovarian cancer.

First, dimensionality reduction and unsupervised clustering analysis were performed on malignant cells from ovarian cancer patients before and after MSLN-KIR CAR-T treatment, dividing the malignant cells into seven clusters. We found that the M3 cluster was significantly increased after treatment and was associated with treatment resistance. Through differential gene intersection analysis, we identified IDO1 as a key gene affecting the efficacy of MSLN-KIR CAR-T in ovarian cancer. IDO1 is the rate-limiting enzyme of tryptophan metabolism, and its main function is to convert tryptophan to kynurenine, thereby creating an immunosuppressive tumor microenvironment. Previous studies have shown that IDO1-mediated metabolic changes may promote tumor immune evasion by depleting local tryptophan, accumulating immunomodulatory metabolites, and altering immune cell signaling [50]. In colorectal cancer, ARID5A enhances CAR-T cell exhaustion by stabilizing IDO1 mRNA, suggesting that IDO1 may be a common mechanism of CAR-T resistance in solid tumors [51]. Recently, in gastrointestinal tumors, IDO1 inhibition has been shown to enhance the efficacy of CLDN18.2-CAR-T, overcoming kynurenine-mediated metabolic suppression [40]. Our findings echo these studies, while for the first time systematically elucidating the function of IDO1 and its upstream regulatory mechanism in the context of ovarian cancer and MSLN-KIR CAR-T. In vitro knockdown and overexpression experiments confirmed the

direct regulatory effect of IDO1 on CAR-T killing function: IDO1 knockdown enhanced CAR-T killing of ovarian cancer cells, whereas overexpression produced the opposite effect. Animal experiments further confirmed that the IDO1-knockdown group exhibited significantly reduced tumor volume and weight and enhanced CAR-T efficacy. These results demonstrate that IDO1 plays a certain role in ovarian cancer treatment resistance.

As a key enzyme in the tryptophan-to-kynurenine (KYN) metabolic pathway, IDO1 catalyzes the metabolism of tryptophan toward KYN. Our study shows that knocking down IDO1 reduces KYN production in ovarian cancer cells, whereas overexpressing IDO1 enhances the conversion of tryptophan to KYN. Further functional experiments demonstrated that exogenous KYN dose-dependently inhibited the killing effect of MSLN-KIR CAR-T cells on tumor cells and increased CAR-T cell apoptosis. These results support the possibility that the IDO1/KYN metabolic axis participates in CAR-T cell function inhibition, and also suggest that tumor metabolites may constitute important microenvironmental factors affecting CAR-T therapeutic efficacy. Yang et al. reported that kynurenine inhibits the expansion and function of CD8 + T cells by inhibiting their glucose uptake, and that 120 μM kynurenine can significantly weaken CAR-T cytotoxicity [52]. Notably, that study enabled CAR-T cells to degrade kynurenine by overexpressing kynureninase, thereby restoring anti-tumor activity in a kynurenine-rich microenvironment. This strategy addresses the kynurenine inhibition problem from the T cell side, whereas our study demonstrates the feasibility of targeting IDO1 to block kynurenine production from the tumor side. At the mechanistic level, the immunosuppressive effects of kynurenine may be achieved through multiple pathways. In addition to directly inhibiting T cell glucose metabolism, kynurenine can also serve as a ligand for the aryl hydrocarbon receptor, activating aryl hydrocarbon receptor signaling and thereby promoting T cell exhaustion [53]. Siska et al. revealed another mechanism of kynurenine action, namely inducing T cell fatty acid oxidation metabolism, thereby altering their metabolic adaptability [54]. These multiple mechanisms may collectively explain the potent inhibition of CAR-T function by kynurenine observed in this study.

Next, we further sought the upstream regulatory mechanism affecting IDO1 expression. Through GSEA analysis of single-cell data, we noticed a significant increase in the glycolysis pathway in the M3 cluster of poor-responder patients before and after treatment. The association between this metabolic feature and IDO1 expression prompted us to explore the possible role of lactylation modification. Lactylation is a newly discovered histone post-translational modification driven by the glycolysis product lactate. Our study is the first to directly link H3K18la to IDO1 transcriptional regulation. First, we noticed that after lactate increase, H3K18la was the most significantly upregulated. ChIP-qPCR experiments demonstrated that H3K18la was enriched in the IDO1 promoter region, and glycolysis inhibitors could attenuate this enrichment. Meanwhile, functional experiments showed that after glycolysis inhibitor treatment, both mRNA and protein levels of IDO1 decreased, whereas increased exogenous and endogenous lactate upregulated IDO1 expression. These data construct a clear regulatory axis: glycolysis produces lactate, lactate drives H3K18la modification, H3K18la enriches in the IDO1 promoter region to activate its transcription, IDO1 then catalyzes the conversion of tryptophan to kynurenine, and kynurenine accumulation ultimately inhibits CAR-T function. Notably, H3K18la epigenetic regulation in ovarian

cancer is not an isolated event. Hu et al. found that LDHB regulates lactate production in ovarian cancer cells, thereby mediating H3K18la modification in the PD-L1 promoter region and activating PD-L1 transcription [55]. Sun et al. reported that lactate activates CCL18 expression in macrophages through H3K18la, promoting ovarian cancer development [56]. This implies that lactate in the tumor microenvironment may simultaneously act on multiple cell types, coordinately creating an immunosuppressive state through H3K18la-mediated transcriptional reprogramming.

p300 has been identified as the major lactyltransferase. P300 has been reported to catalyze H3K18la in other tumor models. In glioma, GTPSCS cooperates with p300 to regulate H3K18la expression, promoting tumor proliferation and radiotherapy resistance [57]. In esophageal cancer, NIPAL1 establishes a metabolic-epigenetic feedback loop through the p300-H3K18la axis, promoting immune evasion [58]. Fang et al. found that p300 is involved in mediating elevated H3K18la levels in atrial fibrillation-related cardiac fibroblasts [59]. Our study extends these findings to ovarian cancer and is the first to verify that p300 regulates IDO1 through H3K18la. First, immunofluorescence and Co-IP experiments confirmed the co-localization and interaction between p300 and H3K18la in ovarian cancer cells. Functional experiments showed that p300 inhibitor or p300 knockdown reduced the enrichment level of H3K18la in the IDO1 promoter region, and p300 inhibitor or p300 knockdown reduced IDO1 expression, while the addition of exogenous lactate could slightly reverse this phenomenon. These results indicate that p300 upregulates IDO1 expression through catalyzing H3K18la.

Based on the above mechanistic findings, we explored the therapeutic effect of the IDO1 inhibitor epacadostat and a p300 inhibitor combined with MSLN-KIR CAR-T for ovarian cancer. Animal experiments showed that CAR-T combined with IDO1 inhibitor or p300 inhibitor significantly inhibited tumor growth, with the triple combination achieving the best effect. Immunohistochemistry confirmed that tumor proliferation was significantly reduced in the combination group. The theoretical basis of this combination strategy is to simultaneously block the catalytic activity of IDO1 and its upstream epigenetic driver. IDO1 inhibitors directly block kynurenine production, while p300 inhibitors inhibit IDO1 expression from the transcriptional source; the combination of the two can achieve a double blockade of this pathway. As a selective IDO1 inhibitor, epacadostat has been tested in multiple clinical trials, and its safety and pharmacokinetic characteristics are relatively well established. Although p300 inhibitors are still in early exploratory stages in tumor therapy, data from this study and other cancer types support their potential as immune therapy sensitizers.

Conclusion

In summary, our research established that IDO1 facilitated tumor immune evasion and treatment resistance in ovarian cancer. It relied on the accumulation of its metabolic product KYN, which in turn suppressed the cytotoxic function and induced apoptosis of CAR-T cells. Mechanistically, lactate accumulation drove p300-mediated H3K18la modification, which activated IDO1 transcription. Consequently, the lactate/p300-H3K18la/IDO1 axis emerged as a promising therapeutic target, and

combined inhibition of p300 and IDO1 provided a viable strategy to overcome resistance to MSLN-KIR CAR-T therapy in ovarian cancer.

Abbreviations

CAR-T: Chimeric Antigen Receptor T-cell

ChIP: Chromatin Immunoprecipitation

DAP12: DNAX Activation Protein 12

E:T ratio: Effector-to-Target ratio

H3K18la: Histone H3 Lysine 18 Lactylation

IDO1: Indoleamine 2,3-Dioxygenase 1

IDO1i: IDO1 Inhibitor

KIR: Killer Cell Immunoglobulin-like Receptor

KYN: Kynurenine

MSLN: Mesothelin

UTD: Untransduced T Cells

Declarations

Acknowledgements

We would like to thank BioGDP and Figdraw for providing drawing templates and materials.

Author Contributions

Su Wang carried out the studies, participated in collecting data, and drafted the manuscript. Zitong Shen and Yuchen Huang participated in analysis of data and drafted the manuscript. All authors read and approved the final manuscript.

Funding

This work was supported by the National Natural Science Foundation of China (Grant Nos. 82372593 and 82573528).

Data Availability

The datasets generated and/or analysed during the current study are available in the Genome Sequence Archive in BIG Data Center. Raw sequencing data are available from Beijing Institute of Genomics (BIG) HRA006416 (https://ngdc.cncb.ac.cn/search/all? &q=HRA006416).

Ethics approval and consent to participate

This study was approved by the Institutional Review Board of The First Affiliated

Hospital of Nanjing Medical University (2021-SR-084). This study adhered to the Declaration of Helsinki. All participants provided written informed consent prior to participation. The animal ethics approval number is ISM-ACUC-AUP-20260433.

Consent for publication

Not applicable.

Competing interests

The authors have declared that no competing interest exists.

References

1. Cabasag CJ, Fagan PJ, Ferlay J, Vignat J, Laversanne M, Liu L, van der Aa MA, Bray F, Soerjomataram I. Ovarian cancer today and tomorrow: a global assessment by world region and human development index using globocan 2020. Int J Cancer. 2022;151(9):1535–41.
2. Soppe SE, Kuo T, Lyratzopoulos G, Derouen MC, Albright BB, Bae-Jump VL, Baggett CD, Wheeler S, Thompson CA. Symptom-related care and diagnoses before ovarian cancer detection: patterns and differences by cancer stage. Gynecol Oncol. 2026;204:100–8.
3. Nayak R, Pandey S, Kumar D, Kumar S, Pai KSR. Signaling networks and mirna crosstalk in ovarian cancer chemoresistance. J Ovarian Res. 2025;18(1):185.
4. Chen B, Liu J. Advances in ovarian tumor stem cells and therapy. Cell Biochem Biophys. 2024;82(3):1871–92.
5. Aryasomayajula C, Johnson CR, Francoeur AA, Sia TY, Darcy KM, Tian C, Kapp DS, Chan JK, Liu YL. Pathogenic germline variants among patients with ovarian cancer by self-reported ancestry: a commercial laboratory collaborative research registry study. Gynecol Oncol. 2026;204:1–8.
6. Malander S, Ridderheim M, Masback A, Loman N, Kristoffersson U, Olsson H, Nilbert M, Borg A. One in 10 ovarian cancer patients carry germ line brca1 or brca2 mutations: results of a prospective study in southern sweden. Eur J Cancer. 2004;40(3):422–8.
7. Poveda A, Floquet A, Ledermann JA, Asher R, Penson RT, Oza AM, Korach J, Huzarski T, Pignata S, Friedlander M, Baldoni A, Park-Simon T, Tamura K, Sonke GS, Lisyanskaya A, Kim J, Filho EA, Milenkova T, Lowe ES, Rowe P, Vergote I, Pujade-Lauraine E. Olaparib tablets as maintenance therapy in patients with platinum-sensitive relapsed ovarian cancer and a brca1/2 mutation

(solo2/engot-ov21): a final analysis of a double-blind, randomised, placebo-controlled, phase 3 trial. Lancet Oncol. 2021;22(5):620–31.

8. Coleman RL, Oza AM, Lorusso D, Aghajanian C, Oaknin A, Dean A, Colombo N, Weberpals JI, Clamp A, Scambia G, Leary A, Holloway RW, Gancedo MA, Fong PC, Goh JC, O'Malley DM, Armstrong DK, Garcia-Donas J, Swisher EM, Floquet A, Konecny GE, Mcneish IA, Scott CL, Cameron T, Maloney L, Isaacson J, Goble S, Grace C, Harding TC, Raponi M, Sun J, Lin KK, Giordano H, Ledermann JA. Rucaparib maintenance treatment for recurrent ovarian carcinoma after response to platinum therapy (ariel3): a randomised, double-blind, placebo-controlled, phase 3 trial. Lancet. 2017;390(10106):1949–61.
9. Matulonis UA, Shapira-Frommer R, Santin AD, Lisyanskaya AS, Pignata S, Vergote I, Raspagliesi F, Sonke GS, Birrer M, Provencher DM, Sehouli J, Colombo N, Gonzalez-Martin A, Oaknin A, Ottevanger PB, Rudaitis V, Katchar K, Wu H, Keefe S, Ruman J, Ledermann JA. Antitumor activity and safety of pembrolizumab in patients with advanced recurrent ovarian cancer: results from the phase ii keynote-100 study. Ann Oncol. 2019;30(7):1080–7.
10. Chung YE, Kim SI, Noh JJ, Lee J, Lee YJ. Immune checkpoint inhibitors for recurrent ovarian clear cell carcinoma: real-world outcomes from a korean multicenter study. Gynecol Oncol. 2025;203:185–90.
11. Noronha MM, de Almeida LFC, Silveira LDHJ, Filho VOC, Friedman Z, Gazzoni GAS, Alves ACF, Veneziani AC. Immune checkpoint inhibitors in clear cell ovarian carcinoma and mixed gynecologic clear cell cohorts: a systematic review and meta-analysis. Int J Gynecol Cancer. 2026;36(6):102863.
12. Jiang F, Guo S, Wang P, Zeng C. Advances in current and emerging immunotherapies for ovarian cancer. Crit Rev Oncol Hematol. 2026;223:105330.
13. Arjumand S, Raj A, Prattay KMR, Omer HBM, Azam F. Chimeric antigen receptor t cell therapy: revolutionizing cancer treatment. World J Clin Oncol. 2025;16(11):108667.
14. Anupindi K, Malachowski J, Hodson I, Zhu D, June CH, Levine BL. The next innovations in chimeric antigen receptor t cell immunotherapies for cancer. Cytotherapy. 2025;27(7):795–811.
15. Maude SL, Laetsch TW, Buechner J, Rives S, Boyer M, Bittencourt H, Bader P, Verneris MR, Stefanski HE, Myers GD, Qayed M, De Moerloose B, Hiramatsu H, Schlis K, Davis KL, Martin PL, Nemecek ER, Yanik GA, Peters C, Baruchel A, Boissel N, Mechinaud F, Balduzzi A, Krueger J, June CH, Levine BL, Wood P, Taran T, Leung M, Mueller KT, Zhang Y, Sen K, Lebwohl D, Pulsipher MA, Grupp SA. Tisagenlecleucel in children and young adults with b-cell lymphoblastic leukemia. N Engl J Med. 2018;378(5):439–48.
16. Su Y, Bao S, Wei YP, Song LJ, Xue YM, Wei XD, Song YP, Yin QS. [Targeted immunotherapy efficacy analysis in patients with relapsed/refractory b cell acute lymphocytic leukemia]. Zhonghua Xue Ye Xue Za Zhi. 2022;43(11):946–51.
17. Chavez JC, Dickinson M, Munoz J, Ulrickson ML, Thieblemont C, Oluwole OO, Herrera AF, Ujjani CS, Lssin Y, Riedell PA, Kekre N, de Vos S, Wulff J, Williams CM, Winters J, Kloos I, Xu H, Neelapu SS.

Three-year follow-up analysis of first-line axicabtagene ciloleucel for high-risk large b-cell lymphoma: the zuma-12 study. Blood. 2025;145(20):2303–11.

18. Ahmed S, Dipersio J, Essell J, Diefenbach C, Perales M, Castilla-Llorente C, Dahiya S, Liu Y, Xu H, Fanton C, Chaudhry S, Lee ZH, Marcondes AMQ, Tagliaferri MA, Zalevsky J, Miklos D, Turtle CJ, Mcguirk J. Nktr-255 enhances complete response following cd19 car t-cell therapy in patients with relapsed/refractory large b-cell lymphoma. Blood Adv. 2025;9(23):6092–5.
19. Arora S, Sethi P, Banerjee A, Akanda MKM, Abd El Hafeez MS, Mehjabin S, Moharir KS, Mohanty S, Sheoran S. Chimeric antigen receptor t-cell therapy for solid tumors: a review of the intricate mechanisms and potential strategies. Int Immunopharmacol. 2026;168(Pt 1):115838.
20. Sirini C, De Rossi L, Moresco MA, Casucci M. Car t cells in solid tumors and metastasis: paving the way forward. Cancer Metastasis Rev. 2024;43(4):1279–96.
21. Qi M, Cattaneo G, Camillo C, Quattrocchi E, Zhang L, Tejeda-Polanco E, Ferrone C, Chen Z, Schwab J. Pitfalls and strategies of car-t therapy in solid tumors and implications for chordoma treatment. Immunotherapy. 2025;17(10):735–47.
22. Zhang B, Wu J, Jiang H, Zhou M. Strategies to overcome antigen heterogeneity in car-t cell therapy. Cells 2025, 14(5).
23. Yoshida Y, Machiyama H, Wakamatsu E, Saito K, Takeuchi A, Nishikawa T, Matsushima R, Nishi W, Nishijima H, Kanno Y, Yokosuka T. Pd-1 suppresses car signaling by forming the inhibitory signalosome colocalizing to car microclusters. Commun Biol. 2026;9(1):135.
24. Johnson A, Townsend M, O'Neill K. Tumor microenvironment immunosuppression: a roadblock to car t-cell advancement in solid tumors. Cells 2022, 11(22).
25. Wang E, Wang L, Tsai C, Bhoj V, Gershenson Z, Moon E, Newick K, Sun J, Lo A, Baradet T, Feldman MD, Barrett D, Pure E, Albelda S, Milone MC. Generation of potent t-cell immunotherapy for cancer using dap12-based, multichain, chimeric immunoreceptors. Cancer Immunol Res. 2015;3(7):815–26.
26. Xu T, Wang C, Chen X, Bai J, Wang E, Sun M. Coexpression of c-jun in multiple-chain dap-car-engineered t-cells for solid tumor therapy. Immunotherapy. 2022;14(18):1457–66.
27. Chen J, Hu J, Gu L, Ji F, Zhang F, Zhang M, Li J, Chen Z, Jiang L, Zhang Y, Shi R, Ma L, Jia S, Zhang Y, Zhang Q, Liang J, Yao S, Hu Z, Guo Z. Anti-mesothelin car-t immunotherapy in patients with ovarian cancer. Cancer Immunol Immunother. 2023;72(2):409–25.
28. Xu T, Tian T, Wang C, Chen X, Zuo X, Zhou H, Bai J, Zhao C, Fu S, Sun C, Wang T, Zhu L, Zhang J, Wang E, Sun M, Shu Y. Efficacy and safety of novel multiple-chain dap-car-t cells targeting mesothelin in ovarian cancer and mesothelioma: a single-arm, open-label and first-in-human study. Genome Med. 2024;16(1):133.
29. Li Z, Wang Q, Huang X, Yang M, Zhou S, Li Z, Fang Z, Tang Y, Chen Q, Hou H, Li L, Fei F, Wang Q, Wu Y, Gong A. Lactate in the tumor microenvironment: a rising star for targeted tumor therapy. Front Nutr. 2023;10:1113739.

30. Chen S, Xu Y, Zhuo W, Zhang L. The emerging role of lactate in tumor microenvironment and its clinical relevance. Cancer Lett. 2024;590:216837.
31. Dai X, Chang J, Wang S, Bentum-Ennin L, Zhou J, Zuo X, Hu W. Beyond a waste product: lactate as a master metabolite dictating anti-tumor t-cell fate. Cell Death Dis 2026, 17(1).
32. Fang C, Zhou S, Yu K, Zhang L, Lian W, Tie X, Chen S, Dai J, Li Q, Wang X. Lactate metabolism and lactylation in cancer: from pathogenesis to therapeutic advances. Signal Transduct Target Ther 2026, 11(1).
33. Hosonuma M, Yoshimura K. Association between ph regulation of the tumor microenvironment and immunological state. Front Oncol. 2023;13:1175563.
34. Gu X, Yang J, Lai R, Zhou Z, Tang D, Hu L, Zhao L. Impact of lactate on immune cell function in the tumor microenvironment: mechanisms and therapeutic perspectives. Front Immunol. 2025;16:1563303.
35. Zhang D, Tang Z, Huang H, Zhou G, Cui C, Weng Y, Liu W, Kim S, Lee S, Perez-Neut M, Ding J, Czyz D, Hu R, Ye Z, He M, Zheng YG, Shuman HA, Dai L, Ren B, Roeder RG, Becker L, Zhao Y. Metabolic regulation of gene expression by histone lactylation. Nature. 2019;574(7779):575–80.
36. Al-Malsi K, Xie S, Cai Y, Mohammed N, Xie K, Lan T, Wu H. The role of lactylation in tumor growth and cancer progression. Front Oncol. 2025;15:1516785.
37. Sun C, Hu D, Peng W, Cui Z, Lin Y. Emerging role of histone and non-histone lactylation in metabolic reprogramming of female-specific malignancies. World J Surg Oncol. 2025;24(1):29.
38. Rab SO, Jaafar HK, Jabir MS, Malathi H, Devi S, Pramanik A, Al-Hetty HRAK, Alnajar MJ, Jawad SF, Mustafa YF. Harnessing ido inhibitors to optimize cancer immunotherapy. Naunyn Schmiedebergs Arch Pharmacol. 2025;398(12):16797–815.
39. Yan J, Chen D, Ye Z, Zhu X, Li X, Jiao H, Duan M, Zhang C, Cheng J, Xu L, Li H, Yan D. Molecular mechanisms and therapeutic significance of tryptophan metabolism and signaling in cancer. Mol Cancer. 2024;23(1):241.
40. Wu Z, Wang H, Zheng Z, Lin Y, Bian L, Geng H, Huang X, Zhu J, Jing H, Zhang Y, Ji C, Zhai B. Ido1 inhibition enhances cldn18.2-car-t cell therapy in gastrointestinal cancers by overcoming kynurenine-mediated metabolic suppression in the tumor microenvironment. J Transl Med. 2025;23(1):275.
41. Huang J, Wang X, Li N, Fan W, Li X, Zhou Q, Liu J, Li W, Zhang Z, Liu X, Zeng S, Yang H, Tian M, Yang P, Hou S. Yy1 lactylation aggravates autoimmune uveitis by enhancing microglial functions via inflammatory genes. Adv Sci (Weinh). 2024;11(19):e2308031.
42. Li F, Si W, Xia L, Yin D, Wei T, Tao M, Cui X, Yang J, Hong T, Wei R. Positive feedback regulation between glycolysis and histone lactylation drives oncogenesis in pancreatic ductal adenocarcinoma. Mol Cancer. 2024;23(1):90.
43. Li W, Zhou C, Yu L, Hou Z, Liu H, Kong L, Xu Y, He J, Lan J, Ou Q, Fang Y, Lu Z, Wu X, Pan Z, Peng J, Lin J. Tumor-derived lactate promotes resistance to bevacizumab treatment by facilitating

autophagy enhancer protein rubcnl expression through histone h3 lysine 18 lactylation (h3k18la) in colorectal cancer. Autophagy. 2024;20(1):114–30.

44. Qin H, Zhou Z, Shi R, Mai Y, Xu Y, Peng F, Cheng G, Zhang P, Chen W, Chen Y, Chen Y, Xu R, Lu Q. Insights into next-generation immunotherapy designs and tools: molecular mechanisms and therapeutic prospects. J Hematol Oncol. 2025;18(1):62.
45. Wang Z, Li P, Zeng X, Guo J, Zhang C, Fan Z, Wang Z, Zhu P, Chen Z. Car-t therapy dilemma and innovative design strategies for next generation. Cell Death Dis. 2025;16(1):211.
46. Hassan R, Remaley AT, Sampson ML, Zhang J, Cox DD, Pingpank J, Alexander R, Willingham M, Pastan I, Onda M. Detection and quantitation of serum mesothelin, a tumor marker for patients with mesothelioma and ovarian cancer. Clin Cancer Res. 2006;12(2):447–53.
47. Okla K, Surowka J, Fraszczak K, Czerwonka A, Kalawaj K, Wawruszak A, Kotarski J, Wertel I. Assessment of the clinicopathological relevance of mesothelin level in plasma, peritoneal fluid, and tumor tissue of epithelial ovarian cancer patients. Tumour Biol. 2018;40(10):1392284727.
48. Ramello MC, Benzaid I, Kuenzi BM, Lienlaf-Moreno M, Kandell WM, Santiago DN, Pabon-Saldana M, Darville L, Fang B, Rix U, Yoder S, Berglund A, Koomen JM, Haura EB, Abate-Daga D. An immunoproteomic approach to characterize the car interactome and signalosome. Sci Signal 2019, 12(568).
49. Long AH, Haso WM, Shern JF, Wanhainen KM, Murgai M, Ingaramo M, Smith JP, Walker AJ, Kohler ME, Venkateshwara VR, Kaplan RN, Patterson GH, Fry TJ, Orentas RJ, Mackall CL. 4-1bb costimulation ameliorates t cell exhaustion induced by tonic signaling of chimeric antigen receptors. Nat Med. 2015;21(6):581–90.
50. Kang I, Theodoropoulos G, Wangpaichitr M. Targeting the kynurenine pathway: another therapeutic opportunity in the metabolic crosstalk between cancer and immune cells. Front Oncol. 2024;14:1524651.
51. Wu D, Wang G, Wen S, Liu X, He Q. Arid5a stabilizes indoleamine 2,3-dioxygenase expression and enhances car t cell exhaustion in colorectal cancer. Transl Oncol. 2024;42:101900.
52. Yang Q, Hao J, Chi M, Wang Y, Xin B, Huang J, Lu J, Li J, Sun X, Li C, Huo Y, Zhang J, Han Y, Guo C. Superior antitumor immunotherapy efficacy of kynureninase modified car-t cells through targeting kynurenine metabolism. Oncoimmunology. 2022;11(1):2055703.
53. Zhu Y, Wang H, Yao Y, Ding H, Xu L, Xu X. Slc1a5-mediated kynurenine metabolism drives ahr-fancd2 axis to remodel chromatin and induce t cell exhaustion in lung adenocarcinoma. Cell Commun Signal 2026, 24(1).
54. Siska PJ, Jiao J, Matos C, Singer K, Berger RS, Dettmer K, Oefner PJ, Cully MD, Wang Z, Quinniii WJ, Oliff KN, Wilkins BJ, Christensen LM, Wang L, Hancock WW, Baur JA, Levine MH, Ugele I, Mayr R, Renner K, Zhou L, Kreutz M, Beier UH. Kynurenine induces t cell fat catabolism and has limited suppressive effects in vivo. EBioMedicine. 2021, 74: 103734.
55. Hu X, Huang Z, Li L. Ldhb mediates histone lactylation to activate pd-l1 and promote ovarian cancer immune escape. Cancer Invest. 2025;43(1):70–9.

56. Sun J, Feng Q, He Y, Wang M, Wu Y. Lactate activates ccl18 expression via h3k18 lactylation in macrophages to promote tumorigenesis of ovarian cancer. Acta Biochim Biophys Sin (Shanghai). 2024;56(9):1373–86.
57. Liu R, Ren X, Park YE, Feng H, Sheng X, Song X, Aminitabrizi R, Shah H, Li L, Zhang Y, Abdullah KG, Dubois-Coyne S, Lin H, Cole PA, Deberardinis RJ, Mcbrayer SK, Huang H, Zhao Y. Nuclear gtpscs functions as a lactyl-coa synthetase to promote histone lactylation and gliomagenesis. Cell Metab. 2025;37(2):377–94.
58. Chen R, Ma X, Xu S, Mo A, Deng M, Wu J, Zhuang W, Duan J, Xie S, Lin J, Lin P, Tang J, Zhou H, Ben X, Qiao G, Xie D. Nipal1 drives a metabolic-epigenetic feedback loop to promote lactate-mediated immune evasion in esophageal cancer. Adv Sci (Weinh). 2026;13(29):e20055.
59. Fang N, Zhang N, Jiang X, Yan S, Wang Z, Gao Q, Xu M, Mu L, Li X, Chen J, Zhang S, Duan Y, Yun F, Li L, Zhang Y, Gong Y. Pfkm-driven lactate overproduction promotes atrial fibrillation via triggering cardiac fibroblasts histone lactylation. Adv Sci (Weinh). 2025;12(34):e963.

Figures

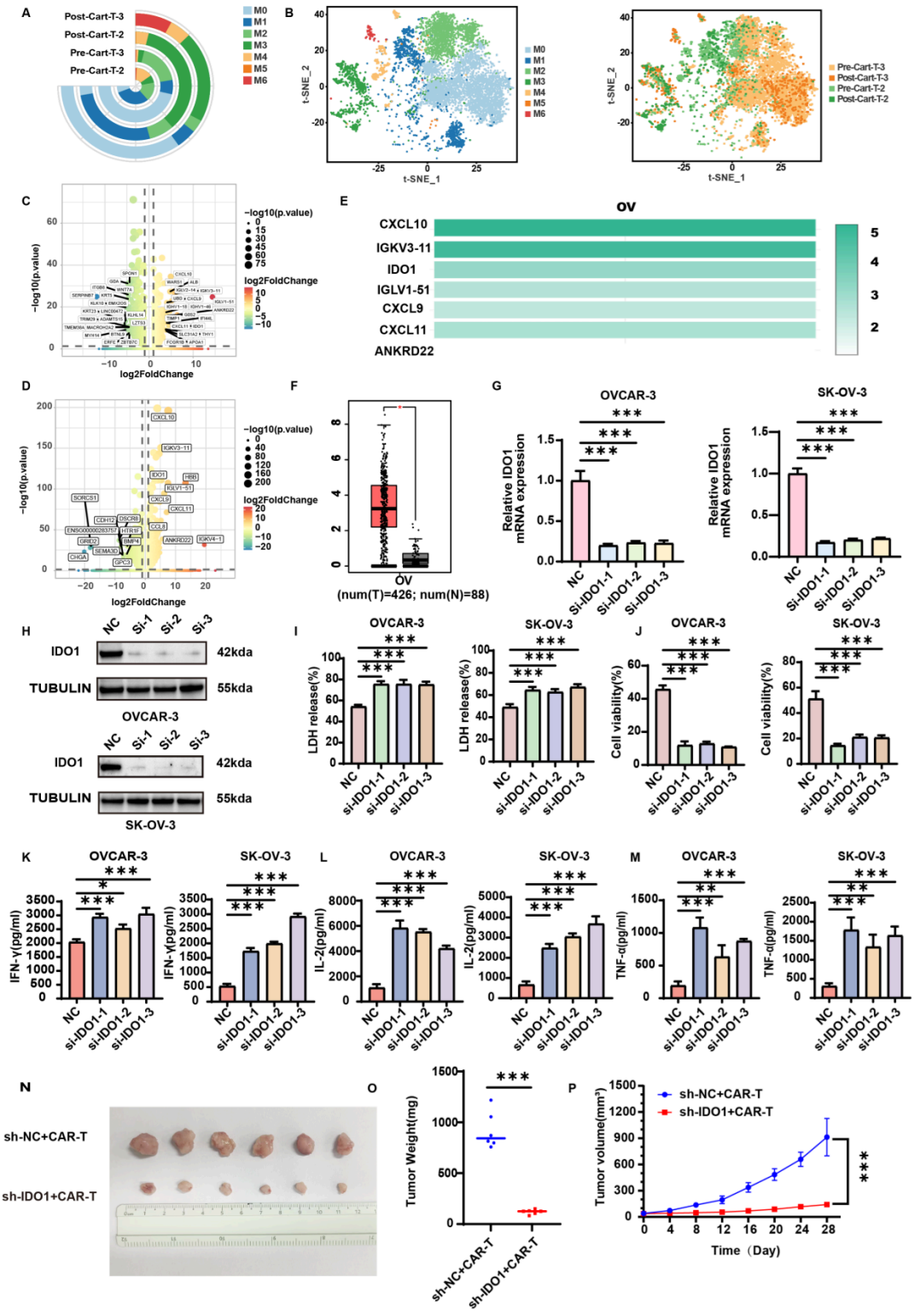

Figure 1

IDO1 potentially promotes resistance to MSLN-KIR CAR-T cell therapy in ovarian cancer patients. *(A) Circos plot showing the distribution proportions of different malignant cells in tumor tissues from ovarian cancer patients before and after CAR-T therapy. (B) t-SNE plot showing the distribution of different malignant cells in tumor tissues before and after CAR-T therapy. (C) Volcano plot showing differentially expressed genes in the M3 cluster before and after treatment; red indicates upregulated genes and blue*

*indicates downregulated genes. (D) Volcano plot showing differentially expressed genes in ovarian cancer patients after treatment compared with before treatment; red indicates upregulated genes and blue indicates downregulated genes. (E) GEPIA online database showing the gene expression levels of CXCL10, IGKV3-11, IDO1, IGLV1-51, CXCL9, CXCL11, and ANKRD22 in ovarian cancer. (F) Box plot showing the differential expression of IDO1 in tumor vs. adjacent normal tissues in ovarian cancer. (G-H) Knockdown efficiency of IDO1 in OVCAR-3 and SK-OV-3 cells detected by RT-qPCR and Western blot. (I-J) The si-NC and si-IDO1 ovarian cancer cell lines were co-cultured with CAR-T cells for 24 h (E:T ratio = 1:1), and LDH and CCK-8 assays were used to detect the cytotoxic effect of CAR-T cells. (K-M) The si-NC and si-IDO1 cell lines were co-cultured with CAR-T cells for 24 h (E:T ratio = 1:1), and the secretion of IFN-γ, IL-2, and TNF-α was detected by ELISA. (N) sh-NC and sh-IDO1 ovarian cancer cells were subcutaneously inoculated into NCG mice (n=6). CAR-T cells were infused 7 days later (day 0), and images of tumors were captured after sacrifice. (O) Tumor weight measured after sacrifice. (P) Tumor volume monitored during the experiment. All data are shown as mean ± SD of three independent experiments. *p < 0.05, **p < 0.01, ***p < 0.001.*

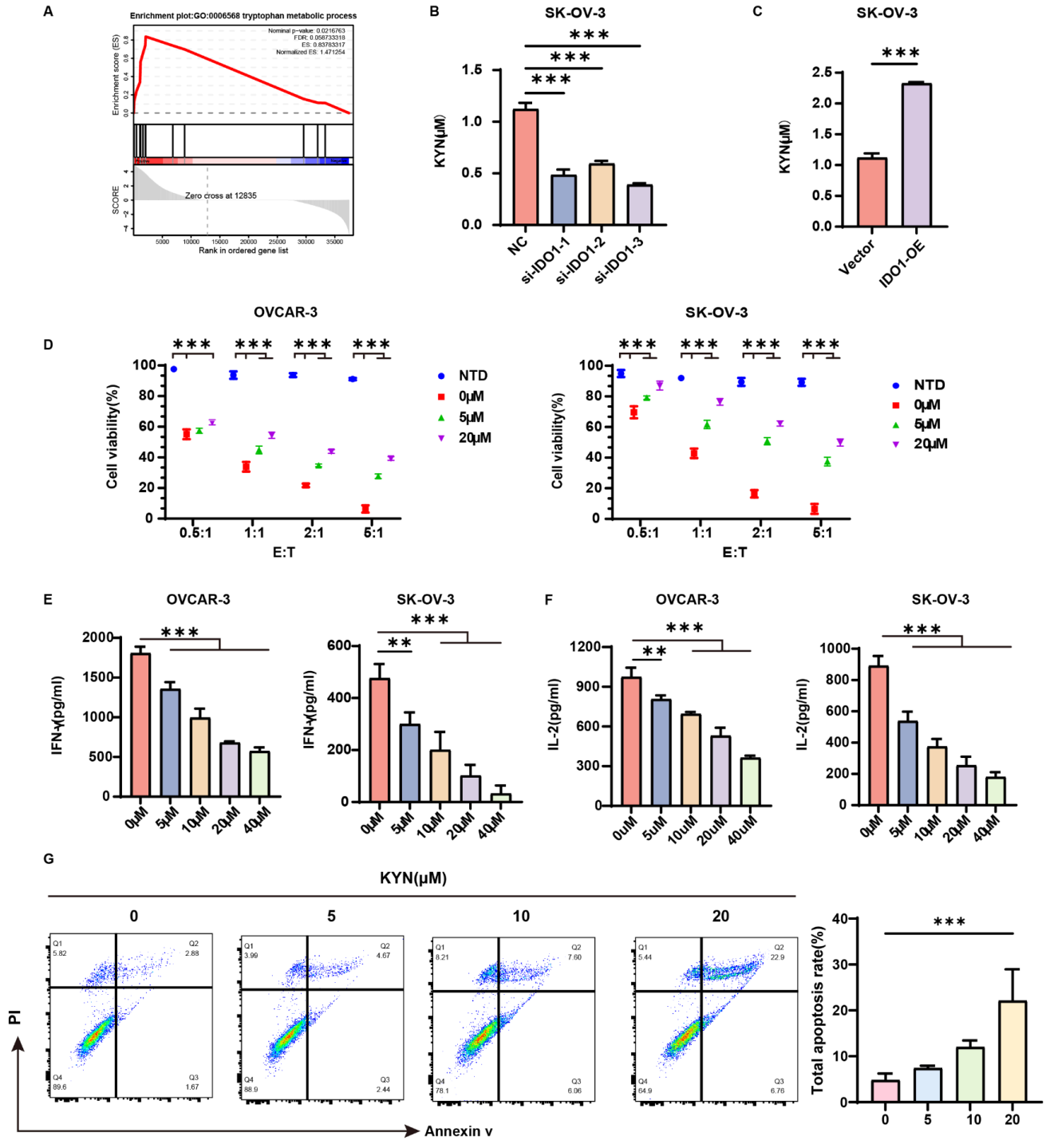

Figure 2

IDO1 metabolizes tryptophan to Kyn, and Kyn suppresses CAR-T cell function. *(A) GSEA of differentially expressed genes in malignant cells from patients before and after treatment. A representative GSEA plot shows enrichment in the tryptophan metabolism pathway (NES = 1.471, P = 0.022). NES, normalized enrichment score; P value, normalized P value. (B) Kyn levels in the supernatant of si-NC and si-IDO1 SK-OV-3 cells detected by ELISA. (C) Kyn levels in the supernatant of Vector and IDO1-OE SK-OV-3 cells detected by*

*ELISA. (D) OVCAR-3 and SK-OV-3 cells were co-cultured with UTD or CAR-T cells at different effector-to-target (E:T) ratios in the presence of different concentrations of Kyn, and the cytotoxic effect of CAR-T cells was assessed by CCK-8 assay. (E-F) OVCAR-3 and SK-OV-3 cells were co-cultured with CAR-T cells (E:T ratio = 1:1) with different concentrations of Kyn, and the secretion of IFN-γ and IL-2 was detected by ELISA. (G) Apoptosis rates of CAR-T cells treated with different concentrations of Kyn for 2 days were detected by Annexin V/PI staining. All data are shown as mean ± SD of three independent experiments. *p < 0.05, **p < 0.01, ***p < 0.001.*

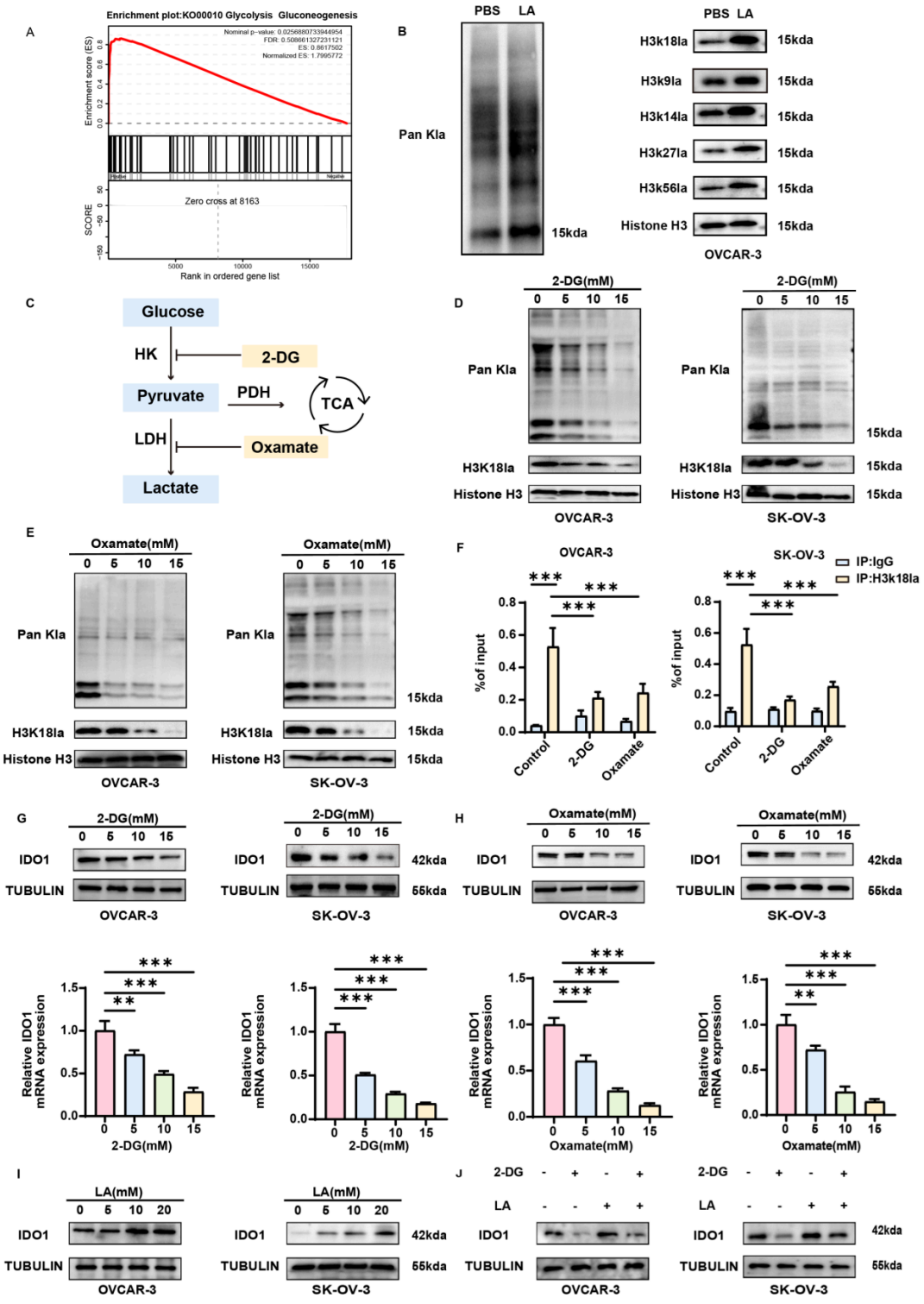

Figure 3

H3K18la activates IDO1 transcription in ovarian cancer cells. *(A) GSEA of differentially expressed genes in the M3 cluster from ovarian cancer patients before and after treatment. A representative GSEA plot shows enrichment in the glycolysis pathway (NES = 1.800, P = 0.026). NES, normalized enrichment score; P value, normalized P value. (B) OVCAR-3 cells were treated with or without lactate (20 mM) for 24 h, and the levels of pan-lactylation and site-specific histone lactylation were detected by Western blot. (C) Schematic diagram of glycolysis and its key target inhibitors. (D-E) OVCAR-3 and SK-OV-3 cells were treated with different concentrations of the glycolysis inhibitors 2-DG and oxamate for 24 h, and the levels of pan-lactylation and H3K18la were detected by Western blot. (F) Ovarian cancer cells were treated with the glycolysis inhibitors 2-DG (10 mM) and oxamate (10 mM) for 24 h. DNA fragments were immunoprecipitated with an H3K18la antibody and analyzed by qPCR. (G-H) Ovarian cancer cells were treated with different concentrations of 2-DG and oxamate for 24 h, and the expression levels of IDO1 were detected by RT-qPCR and Western blot. (I) After OVCAR-3 and SK-OV-3 cells were treated with different concentrations of lactate for 24 h, the expression levels of IDO1 were detected by Western blot. (J) After OVCAR-3 and SK-OV-3 cells were treated with lactate (20 mM) and 2-DG (10 mM) for 24 h, the expression levels of IDO1 were detected by Western blot. All data are shown as mean ± SD of three independent experiments. *p < 0.05, **p < 0.01, ***p < 0.001.*

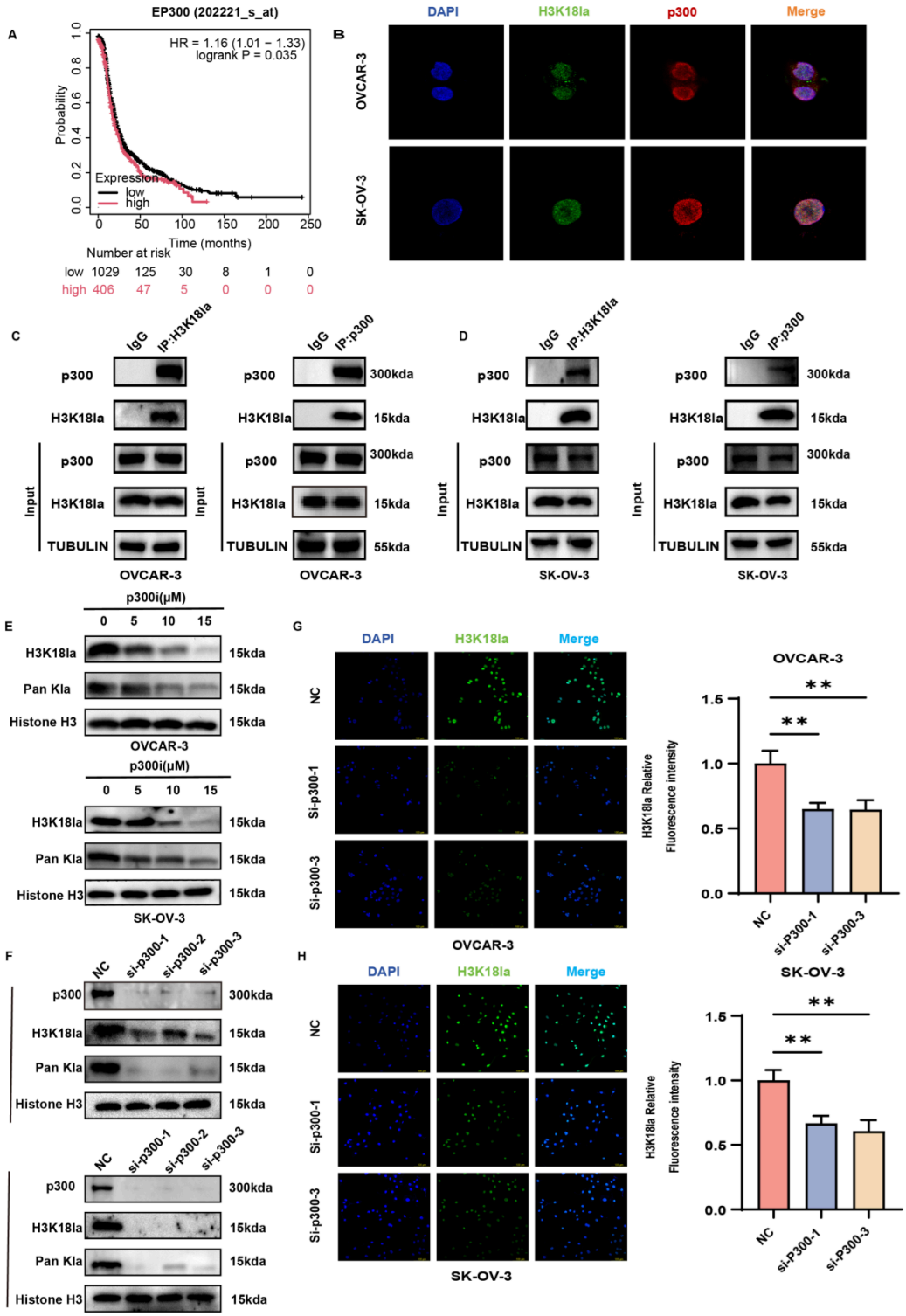

Figure 4

H3K18 is lactylated by p300 in ovarian cancer cells. *(A) Survival analysis of ovarian cancer patients with low and high p300 levels using the GEPIA online database. (B) Immunofluorescence co-staining of p300 and H3K18la in OVCAR-3 and SK-OV-3 cells. (C-D) Co-immunoprecipitation of p300 and H3K18la in OVCAR-3 and SK-OV-3 cells, followed by Western blot analysis. (E) OVCAR-3 and SK-OV-3 cells were treated with different concentrations of a p300 inhibitor, and the levels of pan-lactylation and H3K18la were detected by*

*Western blot. (F) p300 was knocked down in OVCAR-3 and SK-OV-3 cells using siRNA, and the knockdown efficiency as well as the levels of pan-lactylation and H3K18la were detected by Western blot. (G-H) After p300 knockdown, the fluorescence intensity of H3K18la was detected by immunofluorescence (scale bar: 100 μm). All data are shown as mean ± SD of three independent experiments. *p < 0.05, **p < 0.01, ***p < 0.001.*

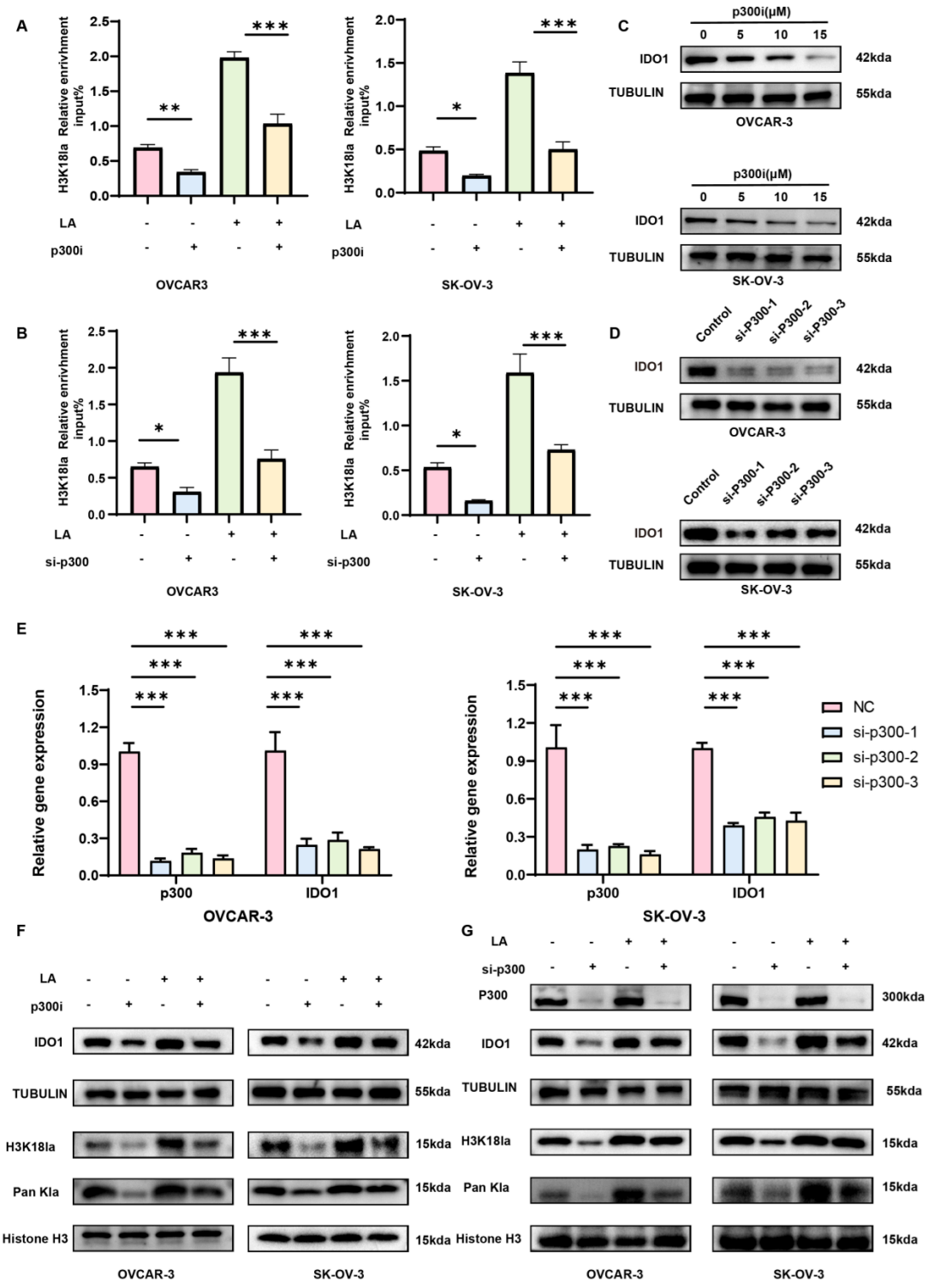

Figure 5

p300 regulates IDO1 expression through H3K18la. *(A) OVCAR-3 and SK-OV-3 cells were treated with a p300 inhibitor (15 μM) or lactate (20 mM), and the enrichment of H3K18la at the IDO1 promoter region was detected by ChIP-qPCR. (B) OVCAR-3 and SK-OV-3 cells were transfected with si-p300 or treated with lactate (20 mM), and the enrichment of H3K18la at the IDO1 promoter region was detected by ChIP-qPCR. (C) Ovarian cancer cells were treated with different concentrations of a p300 inhibitor, and the level of IDO1 was detected by Western blot. (D-E) p300 was knocked down in ovarian cancer cells using siRNA, and the level of IDO1 was detected by qPCR and Western blot. (F) OVCAR-3 and SK-OV-3 cells were treated with a p300 inhibitor (15 μM) or lactate (20 mM), and the levels of H3K18la and IDO1 were detected by Western blot. (G) OVCAR-3 and SK-OV-3 cells were transfected with si-p300 or treated with lactate (20 mM), and the levels of H3K18la and IDO1 were detected by Western blot. All data are shown as mean ± SD of three independent experiments. *p < 0.05, **p < 0.01, ***p < 0.001.*

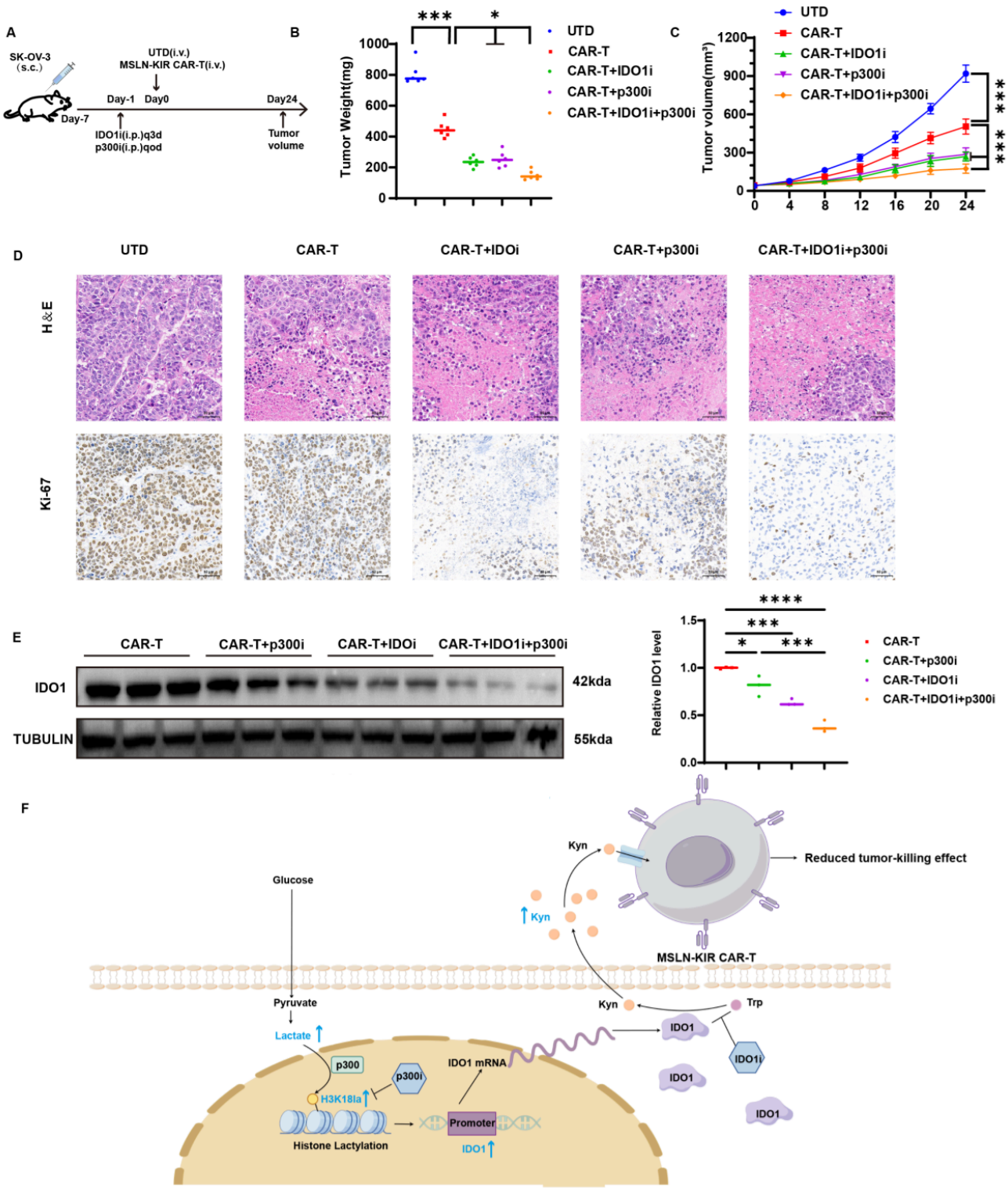

Figure 6

Combined use of MSLN-KIR CAR-T with IDO1i and p300i enhances its therapeutic efficacy against ovarian cancer xenografts in NCG mice.*(A) Schematic diagram of the treatment workflow in NCG mice (Created with BioGDP.com). The antitumor effects of the UTD group, CAR-T group, CAR-T + IDO1i group, CAR-T + p300i group, and CAR-T + IDO1i + p300i group were compared (n=6). (B) Tumor weights in different treatment groups. (C) Tumor volumes in different treatment groups. (D) HE and Ki-67 staining of tumor*

*tissues from different treatment groups (UTD group,CAR-T group, CAR-T + IDO1i group, CAR-T + p300i group, and CAR-T + IDO1i + p300i group). (E) Proteins were extracted from tumor tissues, and the IDO1 protein levels in different treatment groups were detected by Western blot and quantified using ImageJ. (F) Schematic diagram of the mechanism in this study (Created with Figdraw.com). Data are presented as mean ± SD. *p < 0.05, **p < 0.01, ***p < 0.001.*

Supplementary Files

This is a list of supplementary files associated with this preprint. Click to download.

- supplementarymaterials1.docx
- supplementarymaterials2.pdf